CuS/Graphene Nanocomposite as a Transparent Conducting Oxide and Pt-Free Counter Electrode for Dye-Sensitized Solar Cells

JES Focus Issue on Semiconductor Electrochemistry and Photoelectrochemistry in Honor of Krishnan Rajeshwar

CuS/Graphene Nanocomposite as a Transparent Conducting Oxide and Pt-Free Counter Electrode for Dye-Sensitized Solar Cells

Mahyar Mohammadnezhad,[1] Gurpreet Singh Selopal,[1,2,z] Nasser Alsayyari,[1] Rusoma Akilimali,[1] Fabiola Navarro-Pardo,[1,2] Zhiming M. Wang,[2] Barry Stansfield,[1] Haiguang Zhao,[3,z] and Federico Rosei [1,2,*,z]

[1] *Institut National de la Recherche Scientifique, Centre Énergie, Matériaux et Télécommunications 1650 Boul. Lionel Boulet Varennes, Québec J3X 1S2, Canada*
[2] *Institute of Fundamental and Frontier Sciences, University of Electronic Science and Technology of China, Chengdu 610054, People's Republic of China*
[3] *College of Physics & State Key Laboratory of Bio-Fibers and Eco-Textiles, Qingdao University, Qingdao 266071, People's Republic of China*

We report a simple, low temperature and solution-processable approach to prepare a composite film of copper sulfide/graphene (CuS-G) as a transparent conducting oxide (TCO) and platinum (Pt)-free CE for Dye-Sensitized Solar Cells (DSSCs). We find that CuS with 3.3 vol% of graphene (CuS-3G) yields the highest power conversion efficiency (PCE) of 4.83%, which is about 12% higher than DSSCs based on CEs made of pristine CuS. After optimizing the graphene concentration, the PCE of the DSSC assembled with the optimized CuS-3G is comparable to that based on Pt CE. The similar performance of the CuS-3G CE compared with Pt CE is mainly attributed to the small series resistance and high electrocatalytic activity of the CuS-3G CE; this is confirmed by cyclic voltammetry and electrochemical impedance spectroscopy. These results indicate a straightforward methodology for the low cost and easy synthesis of an alternative CE in DSSCs.
 [DOI: 10.1149/2.0121905jes]

Manuscript submitted October 15, 2018; revised manuscript received November 30, 2018. Published December 29, 2018. *This paper is part of the JES Focus Issue on Semiconductor Electrochemistry and Photoelectrochemistry in Honor of Krishnan Rajeshwar.*

The decreasing availability of fossil fuels, which represent over 80% of the world's energy use, dictates an urgent transition toward renewable energy sources.[1–3] In this scenario, solar energy is considered as a promising technology, due to its availability and abundance.[1,2] In the last two decades, dye-sensitized solar cells (DSSCs) have been widely studied due to their promising features, such as cost-effective fabrication technology, large-area scalability and eco-friendliness.[4–7] A DSSC typically consists of a nanocrystalline wide bandgap semiconducting oxide (e.g. ZnO, TiO_2 or SnO_2) mesoporous film deposited on a fluorine doped tin oxide (FTO) transparent conductive glass as electron transporter, dye molecules anchored to the mesoporous film as light harvester, a redox couple electrolyte as hole transport medium, and a platinum (Pt) coated FTO as counter electrode (CE).[8–12]

While the overall fabrication cost of DSSCs is comparatively low, increasing the power conversion efficiency (PCE) and improving long-term stability remain elusive goals for this technology. Several recent efforts have focused on using alternative low-cost nanostructured materials to improve the performance of the different components, specifically the photoanode, the light harvester (dye) and the counter electrode.[13–21] Under light illumination electrons are rapidly excited and injected from the dye molecules into the conduction band of the semiconducting oxide, then transferred to the CE through an external electric circuit to catalyze regeneration of the oxidized iodide/triiodide iodine/iodide redox couple electrolyte.[5,22]

CEs made of Pt coated on the FTO/glass substrate are still the most widely used for the following reasons: (i) they collect electrons from the external circuit and regenerate the oxidized iodide/triiodide redox couple electrolyte at the CE/electrolyte interface, (ii) this material exhibits excellent stability toward the iodide/triiodide redox couple electrolyte, and (iii) its high catalytic activity.[6,23] However, Pt is a costly noble metal and the transparent conductive oxide (TCO) glass commonly used in DSSCs accounts for more than 40% of the total device cost.[22,24,25] Therefore, the design and fabrication of TCO and Pt-free CEs for DSSCs without reducing its electrocatalytic activity represents a major challenge for the commercial deployment of DSSCs.

Different types of materials have been used to fabricate the CE, such as transition metal sulfides, conductive fibers and carbon materials.[6,24–27] Carbon-based materials on FTO substrate showed device efficiencies comparable to a Pt-based CE, due to the low sheet resistance, high catalytic activity and cost-effectiveness.[2,3,18,28] Amongst various carbon materials based CEs, graphene is considered promising due to its outstanding properties such as mechanical strength, high surface area and excellent electrical and thermal conductivity.[2,22,28–30] However, there are still some unresolved issues: reduction in transparency, electrochemical corrosion under persistent cell operation, limited number of active sites for electrolyte electrocatalysis and complicated fabrication processes.[6,24,29,31] To overcome these issues, considerable efforts have recently focused on developing composites made of graphene with functional nanoparticles such as transition metal sulfides, to exploit synergistic effects.[29]

Transition metal sulfides, such as NiS, CoS, CuS, WS and MoS_2, are considered promising materials for potential applications as CEs in DSSCs.[5,22,25,26,29,32] Recently, Patil et al.[26] have developed a low temperature, one pot and solution-processing method to successfully grow a uniform and dense CuS thin film on the FTO substrate. The CE based on the CuS thin film demonstrated good electrocatalytic activity toward the reduction of triiodide. Although the DSSC using the CE based on CuS/FTO thin film exhibits a low PCE compared with the DSSCs based on Pt/FTO CE (28.2% lower), this was the initial step to use low-cost materials and simple processing method for the fabrication of Pt-free CEs.

On the other hand, previous reports indicated that graphene composites can improve the efficiency of the CE through an increase of the electron transfer rate, acting as a spacer between the matrix particles and providing active sites for the electrocatalytic process.[22,28] These reports raise the question of whether graphene composites might also improve the properties of CuS CEs.

As discussed above, numerous previous studies reported transition metal sulfides on FTO substrate as a Pt free CE.[5,22,25,26,29,32] However, the FTO is still one of the most expensive components in DSSCs. Therefore, it is necessary to explore a TCO and Pt-free CEs for

*Electrochemical Society Member.
[z]E-mail: gurpreet.selopal@emt.inrs.ca; hgzhao@qdu.edu.cn; rosei@emt.inrs.ca

Table I. Detailed weight ratio between TAA, CNTH and graphene in the final mixed solution.

Sample	TAA (mg)/ml	CNTH (mg)/ml	G (mg)/ml
CuS	11.28	14.56	0
CuS-2G	11.28	14.56	1.9×10^{-4}
CuS-3G	11.28	14.56	2.9×10^{-4}
CuS-6G	11.28	14.56	5.6×10^{-4}
CuS-10G	11.28	14.56	9.1×10^{-4}

cost effective commercial fabrication of DSSCs. To the best of our knowledge, using a CuS/graphene nanocomposite without using FTO (or other TCO) as the cathode and Pt-free CE in DSSCs has not yet been reported. Here we synthesized CuS/graphene nanocomposite films with varying concentrations of graphene on non-conducting transparent glass and evaluated them as TCO and Pt-free transparent CEs in DSSCs to replace expensive Pt-FTO CEs. The CuS-3G nanocomposite CE exhibits excellent electrocatalytic activity for electrolyte reduction and a comparable PCE (4.83%) to that based on conventional Pt CEs (5.14%).

Experimental

Materials.—Anatase TiO_2 paste with nanoparticle size of 20 nm (18 NR-T) and anatase TiO_2 scattering paste of 150–250 nm nanoparticles (WER2-O) were purchased from DyeSol. The TiO_2 blocking layer solution (Ti-nanoxide) and Ru-based molecular complex dye N719 were purchased from Solaronix. Copper nitrate trihydrate (CNTH) [$Cu(NO_3)_2 \bullet 3H_2O$], thioacetamide (TAA) (C_2H_5NS), acetone and ethanol were obtained from Sigma-Aldrich. All materials were used as received, without any further purification. Graphene microplatelets were purchased from Cheaptubes.

CE fabrication.—Glass substrates were ultrasonically cleaned first in acetone and then in isopropanol for 20 minutes each, then dried with nitrogen gas. The coating solution was prepared by dissolving 3 mmol of copper nitrate trihydrate in 25 mL ethanol and sonicating in a water bath for 40 minutes. Additionally, 7.5 mmol of thioacetamide was dissolved in 25 mL ethanol and sonicated in water-bath for 30 minutes. Then, the thioacetamide solution was added to the copper nitrate trihydrate solution. After 2.5 hours of sonication, the mixed solution color changed to dark green-blackish. The graphene suspension was prepared by adding 10 mg of graphene powder to 20 mL ethanol, followed by sonicating in a water bath for three hours to ensure homogeneity of the solution. Subsequently different volume percentages of the graphene suspension were added to the prepared CuS solution: CuS-2G (2 vol%), CuS-3G (3.3 vol%), CuS-6G (6.6 vol%), CuS-10G (10 vol%) (Table I). The final solution was then sonicated in water bath for 30 minutes. The pre-cleaned glass substrates were submerged into the solution inside a glass tube, tilted at an angle of 45–60 degrees. The glass tube was carefully closed to prevent overflow and was kept in a water bath maintained at 95°C for 2 hours. The film was formed on the bottom-facing side of the glass. The coated substrate was then sintered at 100°C for 15 minutes to ensure removal of all organic substances. The Pt coated FTO/glass substrate CEs with 10 nm thickness were prepared using a RF magnetron sputtering system (Kurt J. Lesker, CM818) under argon atmosphere.

Device fabrication.—Fluorine-doped tin oxide (FTO) glass substrates were first washed thoroughly with water and soap, then sonicated in acetone and isopropanol, respectively, for 20 minutes, subsequently dried with nitrogen gas, and finally irradiated with UV for 20 minutes. The clean FTO substrates were spin-coated with the blocking layer in a single step (rotation speed of 6000 rpm with acceleration of 2000 rpm^2 for 30 s), followed by annealing at 500°C for 30 minutes under ambient air conditions. The TiO_2 paste was then deposited on top of the blocking layer using the tape cast method, as reported previously.[15,16] The substrates were subsequently annealed at 500°C for 30 minutes under ambient air conditions. After that, the photoanodes were dye-loaded by immersing them into a 0.5 mM ethanolic solution of commercial Ru-based molecular complex N719 dye for 24 hours, and then washed gently with ethanol and let dry in ambient air. The DSSC devices were fabricated by using an I^-/I^{3-} redox couple electrolyte and sealed with a 60 μm thick thermal-plastic spacer (Meltonix 1170-60PF, Solaronix). The electrolyte mixture consisted of 1,2-dimethyl-3-propylimidazolium iodide, iodine and acetonitrile that was purchased from GreatCell Solar (MS Code: MS005615).

Characterization.—The morphology of the films was characterized by scanning electron microscopy (FE-SEM, JEOL JSM-6900 F) equipped with an energy-dispersive X-ray spectrometer (EDS), and atomic force microscopy (AFM, Veeco Enviroscope). The crystallinity of the CuS films was investigated using grazing incidence X-ray diffraction (GIXRD) in a Bruker D8 Advance X-ray diffractometer equipped with Cu K_α radiation. Cyclic voltammetry (CV) was carried out in a Solartron SI 1287 potentiostat galvanostat using a three-electrode system (with different CuS-G samples as working electrode, Ag/AgCl reference electrode and a Pt plate as counter electrode) in diluted I^-/I^{3-} redox couple electrolyte in acetonitrile (20 times), at a scan rate of 10 mVs^{-1}. Electrochemical impedance spectroscopy (EIS) was carried under dark conditions using a SOLARTRON 1260 A by applying bias voltages of 0 to 200 mV. Impedance measurements were fitted and analyzed using an appropriate equivalent circuit model with Z-View software. XPS was performed in a VG Escalab 220i-XL equipped with an Al K_α source. The current density-voltage (J-V) characteristic of the cell was obtained using a Keithley 2400 Source Meter under simulated sunlight with an ABET2000 solar simulator at AM 1.5G (100 mW cm^{-2}).

Results and Discussion

Figure 1a displays a photograph of the CuS-G composite film coated on the glass substrate, which exhibits a slightly greenish color and highlights the film homogeneity and transparency. Figures 1b–1g shows the SEM images at different magnifications of hydrothermally grown bare CuS and CuS-G hybrid nanocomposite films on the glass substrate with different contents of graphene. As observed in these images, the CuS film was homogenously grown on the glass substrate after a two-hour hydrothermal reaction. The hydrothermally grown CuS film is composed of continuous and uniform crystalline grains with an average diameter of ~0.34 μm and standard deviation = 0.014. As displayed, the microstructure of bare CuS (Figures 1b–1c) and CuS-3G (Figures 1d–1e) are similar and homogenous (completely crack-free). However, it is quite challenging to detect graphene due to the very low concentration and uniform distribution of the graphene sheets between the CuS nanoparticles. On the other hand, the surface of the CuS-10G film exhibits deep cracks and holes (Figures 1b–1c). These results suggest that the high graphene concentration in the CuS precursor causes the formation of extended micro-cracks, likely due to the strong Van der Waals interaction between carbon sheets resulting in agglomeration.[33] The formation of these defects can reduce the electron transport and electrocatalytic properties of the CE.[2,18,28] This was further verified by carrying out photovoltaic and carrier dynamics characterization of DSSCs assembled by using CuS-10G CEs (see Figure 2 and Figure 3).

To investigate the effect of the CE on the PV performance of the DSSCs, we fabricated five series of DSSCs based on CuS-graphene nanocomposite CEs. Initially, we investigated the effect of graphene concentration in the CuS thin film CE. Figure 2a displays the J-V curves obtained under one sun simulated sunlight at AM 1.5G (100 mW cm^{-2}) of DSSCs with CuS CEs with different concentrations of graphene. The calculated PV parameters, including the open-circuit voltage (V_{oc}), short circuit current density (J_{sc}), fill factor (FF) and PCE of the corresponding devices are summarized in Table II. The results show that initially the PCE improves by increasing the graphene concentration. The best PCE was found to be 4.83%

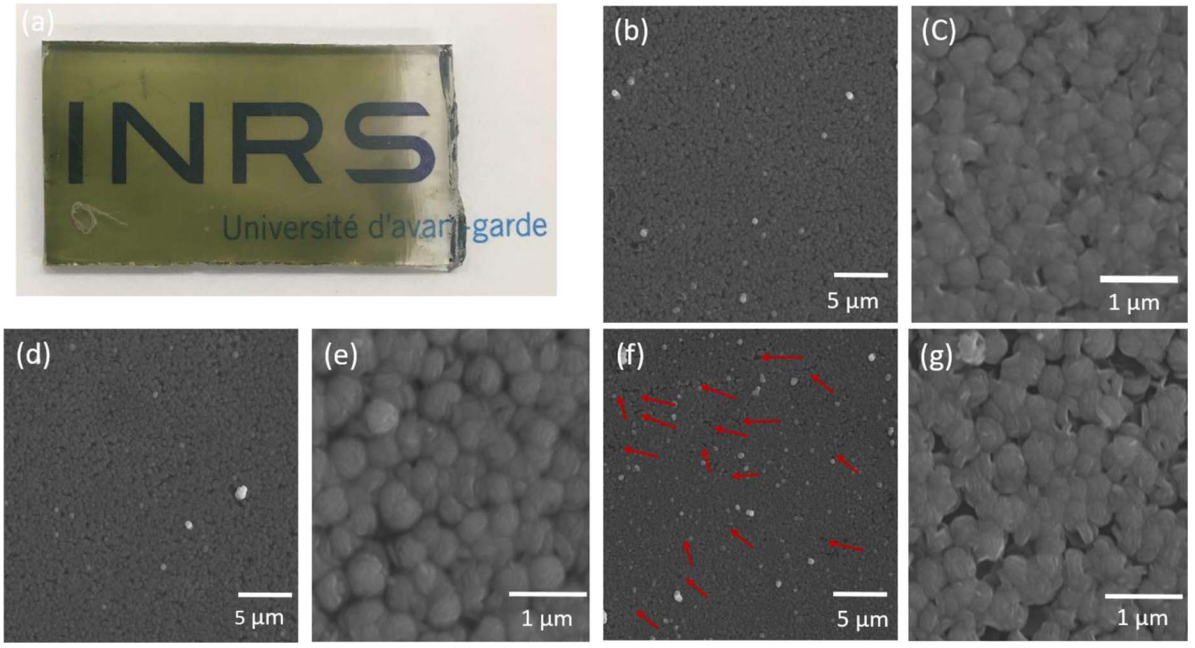

Figure 1. (a) Photograph of the CuS-G composite film. SEM images of CuS film with different concentrations of graphene at different magnifications: (b)-(c) bare CuS-0G; (d)-(e) CuS-3G; (f)-(g) CuS-10G. Red arrows highlights the microcrack areas.

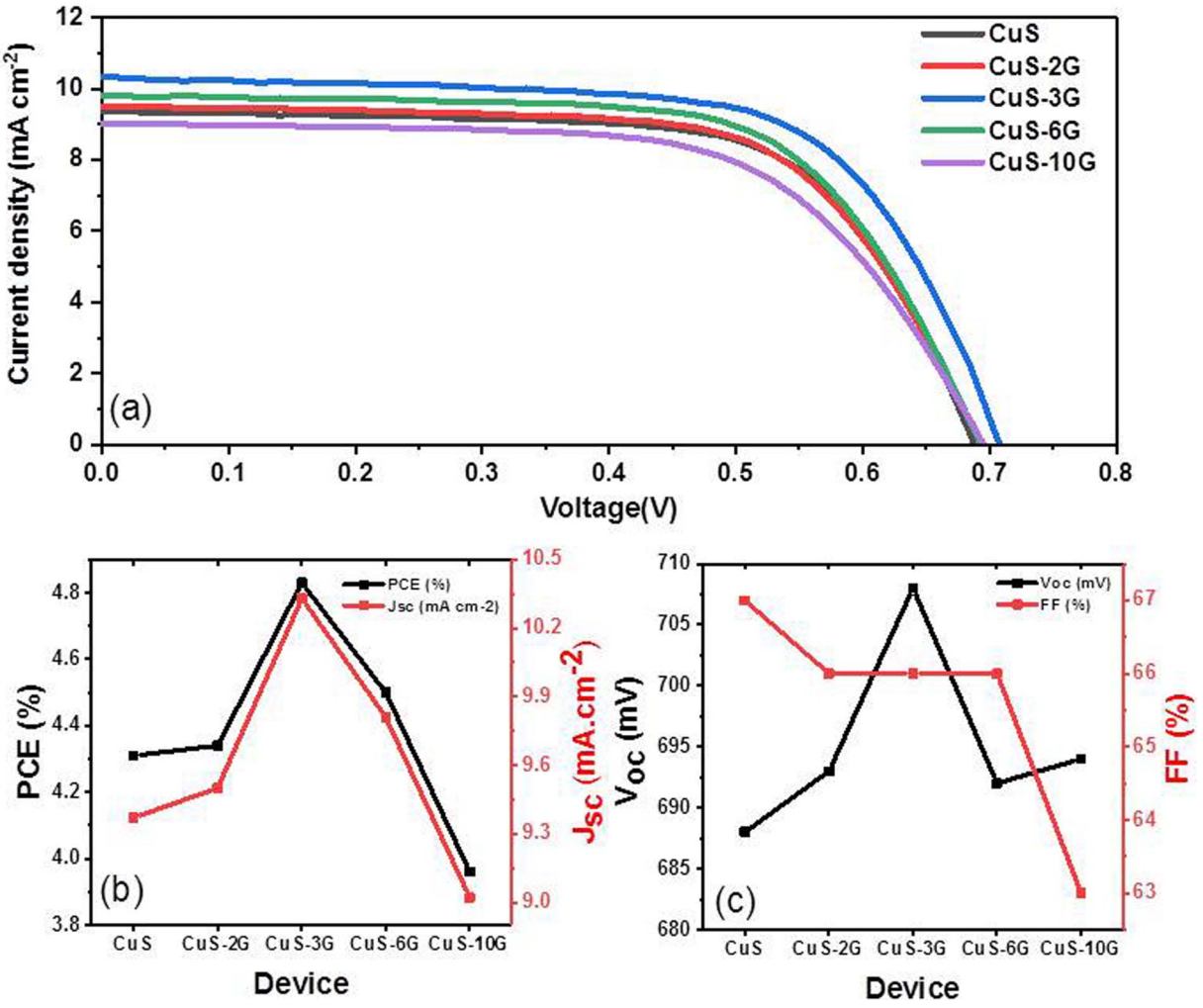

Figure 2. (a) Current density-voltage curves of the solar cells under one sun simulated sunlight at AM 1.5G (100 mW cm^{-2}) fabricated using different CuS-G nanocomposite CEs. Variation of the photovoltaic parameters of the corresponding devices: (b) PCE (%) and J_{sc} (mA.cm^{-2}); (c) V_{oc} (mV) and FF (%).

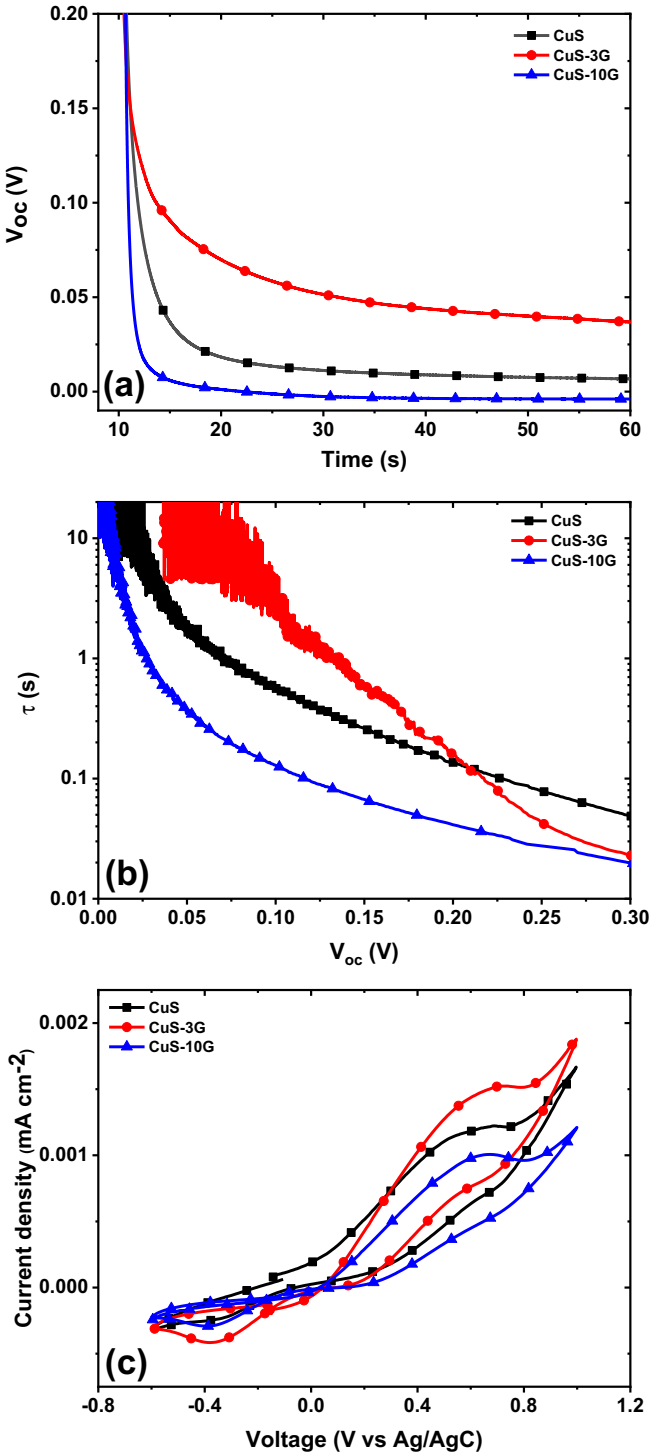

Figure 3. (a) Transient photovoltage decay and (b) electron lifetime for DSSCs fabricated using different CEs. (c) Cyclic voltammogram of different CEs.

for DSSCs made with the GuS-3G composite CE compared to 4.31% for bare CuS. The moderate increase in performance is mainly attributed to the increased functional parameters, mainly J_{sc} and V_{oc} in the optimized solar cell, as displayed in Figures 2b–2c. The increase in J_{sc} and V_{oc} can be attributed to the effective dispersion of graphene amongst the CuS nanoparticles.[22,29] The increase in the contact area of the CE/electrolyte is another effect that can improve the J_{sc} (discussed later).[5,22,24] The high surface area and conductivity of the

Table II. Functional parameters of DSSCs fabricated using different CuS-G nanocomposite CEs.

Sample	PCE (%)	FF (%)	V_{oc} (mV)	J_{sc} (mA.cm^{-2})
CuS	4.31	67	688	9.37
CuS-2G	4.34	66	693	9.50
CuS-3G	4.83	66	708	10.33
CuS-6G	4.50	66	692	9.81
CuS-10G	3.96	63	694	9.02

CE can improve the electrocatalytic activity for faster triiodide electrolyte reduction.[5] The device with CuS-10G CE exhibits a much lower PCE (3.96%) than that of the CuS-3G based DSSCs (4.83%). This may be mainly ascribed to the lower J_{sc}, V_{oc} and FF, which originates from the non-uniform CuS thin film (that shows some deep cracks and holes) on the glass substrate (Figures 1f–1g). The CE not only serves as a superior catalyst for reducing electrolytes but also as a conducting film for electron collection from the external circuit.[2,18,28] Therefore, to obtain high efficiency DSSCs, a good quality film without defects (especially cracks and holes) and high surface area is necessary for electron transfer, catalytic reaction and fast regeneration of the oxidized electrolyte.[23] J-V results indicate that the composite film CuS-3G exhibits higher PV performance than the bare CuS. On the other hand, further increasing the concentration of graphene decreased the PV parameters, which could be related to defect formation in the film.

According to Durrant's report,[34] the optimization of the electrode structure to improve recombination resistance and electron lifetime is a crucial factor to increase the PV performance of DSSCs. DSSCs were illuminated with one sun simulated sunlight (AM 1.5 G, 100 mW cm^{-2}) for ten seconds to reach a steady voltage (V_{oc} of the device). Then, the light was turned off and the voltage decay versus time was recorded under dark conditions. The photovoltage decay of DSSCs based on CuS-G nanocomposite CEs with different concentrations of graphene is shown in Figure 3a. The photovoltage decay rate is lowest for DSSCs based on CuS-3G CE and highest for CuS-10G CEs. The recombination process and electron lifetime (τ_e) of the DSSCs are investigated using transient photovoltage decay that can be defined using Equation 1:[35]

$$\tau_e = -\left(\frac{k_B T}{e}\right) / \left(\frac{dV_{oc}}{dt}\right)$$

where T is the absolute temperature, k_B is Boltzmann's constant, and e is the elementary charge. The calculated τ_e curves of DSSCs based on CuS-G nanocomposite CEs with different concentrations of graphene are shown in Figure 3b. At a particular value of V_{oc} (0.15 V), the calculated τ_e follows the trend: CuS-3G > CuS-0G > CuS-10G, which is consistent with the obtained PV performance of the corresponding devices. This difference in τ_e is mainly attributed to the electrocatalytic properties of the CEs, as all other components of the device were same. The highest τ_e of the DSSCs based on CuS-3G are due to the defect free film (especially a lack of cracks and holes) and high surface area. On the other hand, the devices based on CuS-10G CE show a shorter lifetime compared to the case of bare CuS. In the CuS-10G sample, the addition of a large amount of graphene causes a sharp decline of the electron lifetime. This reduction of the electron lifetime on the DSSC based on CuS-10G CE could be related to defect formation that can hinder electron transport, resulting in very large electron recombination, in agreement with J-V results.

CV is a very powerful technique to evaluate the catalytic activities of the prepared CEs. All the CV curves were obtained in the standard three-electrode system composed of a working electrode (our CuS, CuS-3G and CuS-10G CEs), Pt plate as counter electrode, and Ag/AgCl as reference electrode. The CV spectra for the CuS, CuS-3G and CuS-10G CEs are shown in Figure 3c. The CV curves exhibit two pairs of redox peaks. The one at more negative potentials corresponds to the reduction of triiodide ($I_3^- + 2e^- \rightarrow 3I^-$) and the other at

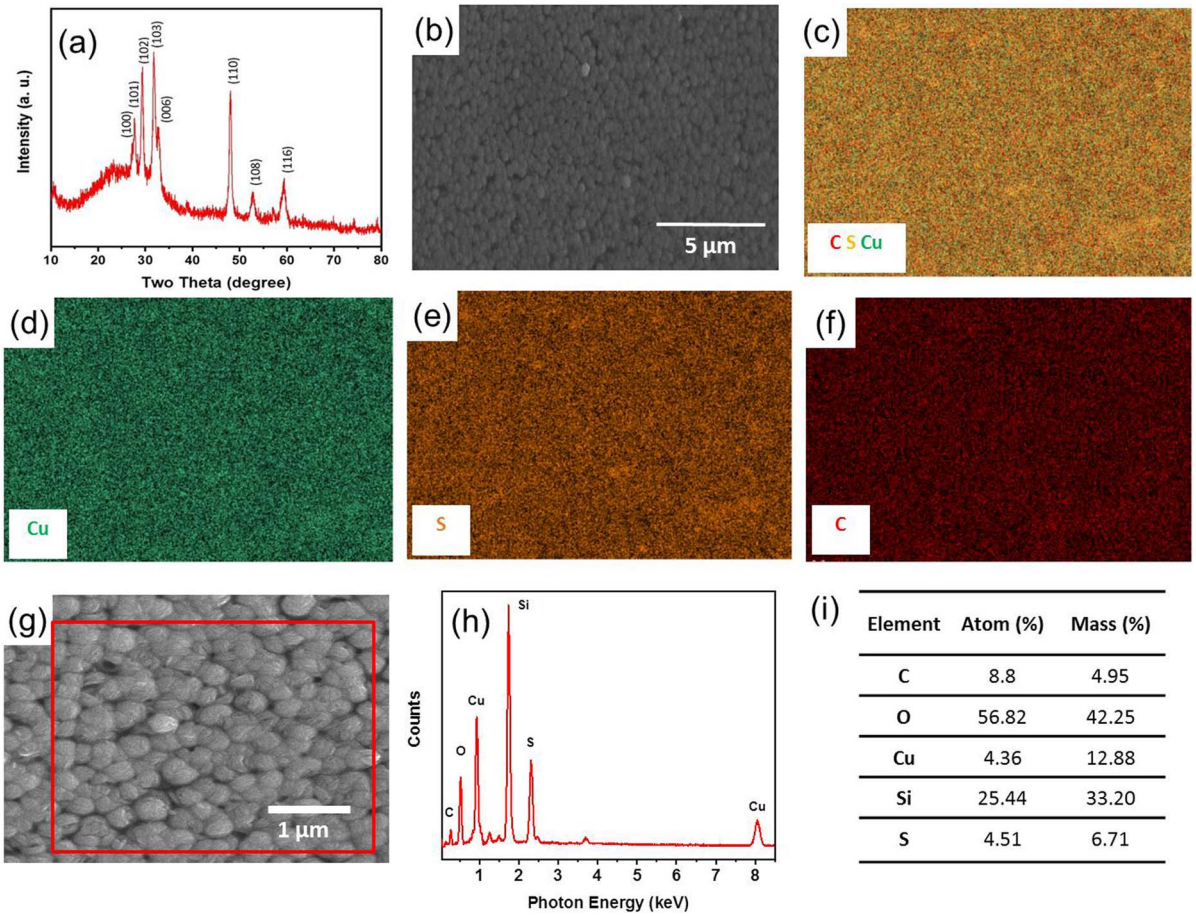

Element	Atom (%)	Mass (%)
C	8.8	4.95
O	56.82	42.25
Cu	4.36	12.88
Si	25.44	33.20
S	4.51	6.71

Figure 4. (a) XRD pattern of as-prepared CuS-3G nanocomposites. EDS images of selected area of (b): (c) C, S, Cu; (d) Cu; (e) S; (f) C. (h-i) EDS mapping and measurement of chemical composition taken from the red squared zones marked in (g).

more positive potentials relates to the oxidation of the iodide ($3I^- \rightarrow I_3^- + 2e^-$).[32,36] As can be observed, the CuS-3G film on the glass substrate represented a higher specific current density per unit area when compared to the CuS, which may be attributed to the higher electrical conductivity of the graphene composite sample.[18,24,37] The reduction of triiodide is faster with the CuS-3G nanocomposite as compared to CuS and CuS-10G, indicating strong electrocatalytic ability of the CuS-3G composite sample.[27] Compared with the CuS and CuS-3G CEs, the current density of CuS-10G is the lowest, due to its poor electrocatalytic ability, as confirmed by the CV measurements (see Figure 3c). The reduced electrocatalytic activity of the CuS-10G CE can be attributed to not only the lower electrical conductivity, but also the lesser active surface area of the non-uniform CuS-10G thin film that exhibits deep cracks and holes (see Figure 1g) as compared to CuS and CuS-3G CEs. The CE with poor catalytic performance has over potential for electron transfer from the external circuit to the electrolyte which enhances electron-hole recombination events.[22–25] This is consistent with the differences in the PV performance of DSSCs based on CuS, CuS-3G and CuS-10G CEs.

The crystalline structure of best performing CuS based CE (CuS-3G nanocomposite) was characterized by XRD. The diffraction pattern displays eight characteristic peaks at 2-theta values 27°, 27.7°, 29.3°, 32.7°, 47.9°, 52.6°, 59.4°, which correspond to the crystal planes of (1 0 0), (1 0 1), (1 0 2), (1 0 3), (0 0 6), (1 1 0), (1 0 8), (1 1 6), respectively (Figure 4a). All peaks matched well with the values in the standard card of CuS (JCPDS 06-0464). This confirms that the CuS particles are the main constituent of the CuS-3G composite film.[26,38] We did not identify any diffraction peak corresponding to graphene. In addition, the energy dispersive X-ray spectroscopy (EDS) spatial images of the corresponding CuS-3G composite film (Figure 4b) are displayed in Figures 4c–4f. The EDS analysis confirms the uniform distribution of Cu, S and C on the sample surface. The peaks of different elements in the selected zones (red square in Figure 4g) are shown in the EDS spectrum. The elemental quantitative data indicates that the Copper to Sulfur ratio is consistent with the chemical Cu/S ratio of CuS. In addition, this measurement confirms the formation of the CuS-G nanocomposite by the presence of the carbon peak, which relates to the graphene content. The oxygen and silicon content in the EDS spectra originate from the glass substrate. These results confirm the excellent crystallinity of CuS in CuS-3G composites and homogeneous dispersion of graphene sheets.[39,40]

XPS analysis was carried out to obtain more detailed information on the surface chemical composition of the CuS-3G nanocomposite film. As shown in Figure 5a, the survey spectrum shows that the film was composed of C, O, S and Cu without any extra peak related to impurities. To further evaluate the chemical bonding of the elements, C, Cu and S peaks were investigated by acquiring high resolution spectra. The C1s spectrum can be de-convoluted into four different peaks (Figure 5c). The main peak at 284.7 eV can be attributed to C-C and C=C bonds. The peaks at 286.5, 288.4 and 289.9 eV are assigned to carbon atoms bound to oxygen atoms by a single bond and by a double bond.[5,37–39] High-resolution XPS spectra of Cu 2p shows two peaks attributed to the doublet Cu $2p_{3/2}$ and Cu $2p_{1/2}$ at 932.1 and 952.1 eV, respectively are shown in Figure 5b. The weak shake-up satellite line at approximately 942.5 eV is also visible. All the Cu peaks are assigned to Cu (II) in CuS.[38,41] The Auger line of Cu at 568.3 eV, which is the typical binding energy value for CuS, indicates that there is a small amount of Cu(I) (Figure 5d).[40] The corresponding XPS spectrum of S2p can be fitted with two main peaks that are $S2p_{3/2}$

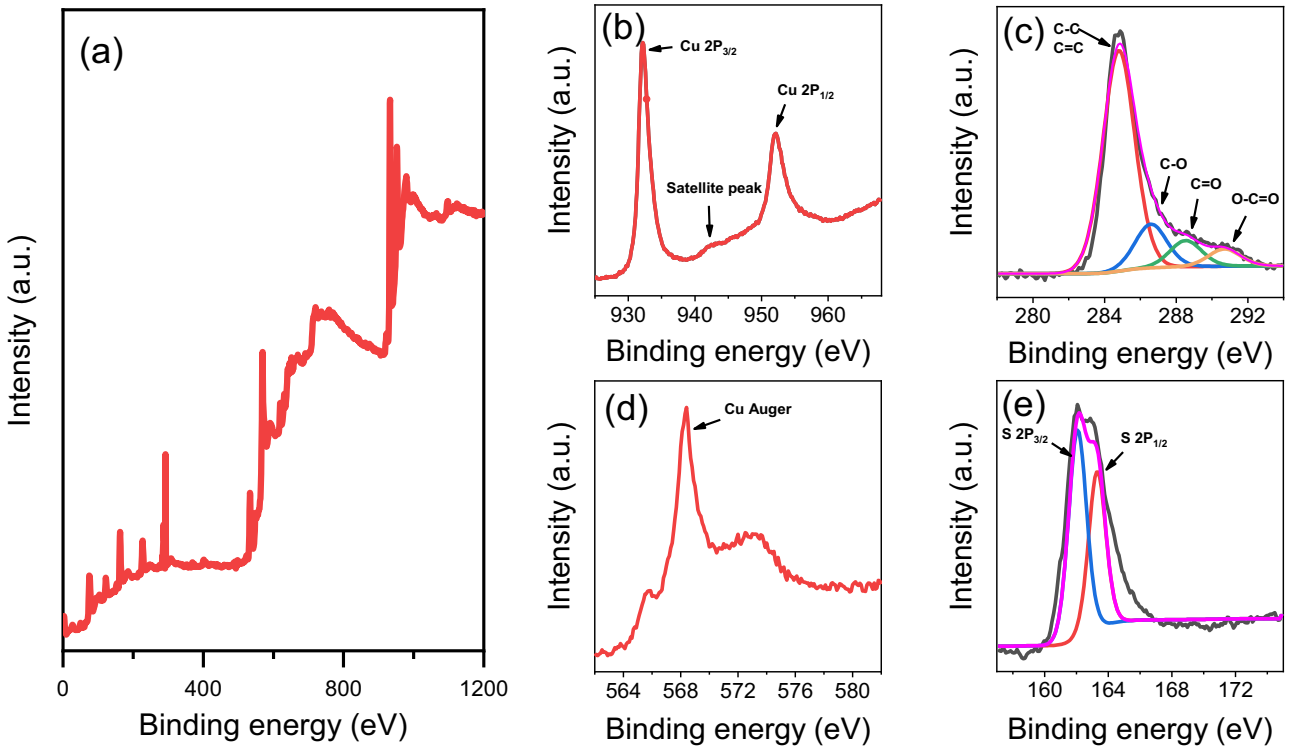

Figure 5. XPS plots of the CuS-3G composite film: (a) Survey, (b) Carbon, (c) Cu, (d) Auger Cu and (e) Sulfur.

at 162 eV and S2p$_{1/2}$ at 163.3 eV, which is a typical value for metal sulfides (Figure 5e).[38,41] The XPS data are well matched with the reported values and support the XRD results that a nanocomposite CuS-graphene film has been successfully synthesized on the glass substrate.[29,39–41]

A deeper understanding of the functional properties of the CEs was obtained by comparing the performance of the DSSCs based on the Pt and optimized CuS-3G CEs. Figure 6a, illustrates the comparison of the J-V curves obtained under one sun simulated sunlight at AM 1.5G (100 mW cm^{-2}) of DSSCs based on Pt and CuS-3G CEs. The results show that the device with an optimized CuS-3G nanocomposite CE on the glass substrate yields a PCE of 4.83%, which is comparable to the PCE of DSSCs based on platinized FTO CEs (5.14%). DSSCs based on Pt and CuS CEs exhibit a similar FF, 67% and 66% respectively, as a result of the high electrocatalytic properties of CuS (Table III).[32] However, a slightly higher photocurrent density was obtained for the Pt CE (10.86 mA.cm^{-2}) than for the device based CuS-3G CE (10.33 mA.cm^{-2}). The CuS based CE on the glass substrate demonstrates a transparent behavior (Figure 1a), while the Pt sputtered CE shows a mirror-like surface with high reflectivity. Hence, the Pt CE is expected to reflect the unabsorbed portion of the incident solar light back to the photoanode and thus enhance the light-harvesting efficiency of the DSSCs.[36] This might be a possible reason for the higher J_{sc} value in the device based on Pt CE than the device based on the CuS-3G CE. The V_{oc} was found to be similar (~700 mV) for the two devices.

Table III. Functional parameters of DSSCs with different Pt and CuS-3G CEs.

Sample	PCE (%)	FF (%)	V_{oc} (mV)	J_{sc} (mA.cm^{-2})
Pt	5.14	67	702	10.86
CuS-3G	4.83	66	708	10.33

The electrocatalytic properties of the Pt and CuS-3G CEs were investigated by using CV and EIS analysis. Figure 6b presents CV curves of the Pt and CuS-3G CEs for the iodide/triiodide electrolyte. The CV curves acquired for the two samples exhibit two pairs of redox peaks. The anodic and cathodic peak separation of the platinized FTO was slightly less than that of the CuS-based electrodes. However, the current densities in the redox peaks of the CuS-3G composite film are higher than those of the Pt, indicating that the synthesized electrode exhibits excellent electrocatalytic activity as the CE in a DSSC system. This may be attributed not only to the higher electrical conductivity of the graphene composited sample, but also to the improved surface area from the higher surface roughness (discussed later in more detail).[18,24,37]

To further confirm the investigation on the electrocatalytic activity of CEs from the CV results, the EIS analysis was carried out in two identical cells with Pt and CuS-3G CEs, as shown in Figures 6c–6e. The intercept of the semicircle on the real axis is assigned to the series resistance (R_s), which is very close for the two CEs under various applied voltages (Figure 6d). Besides the R_s, the charge transfer impedance (R_{ct}) of the counter electrode is another important parameter which affects the performance of DSSC that can be obtained from EIS. R_{ct} can be assigned to the impedance of the charge transfer process occurring at the counter electrode and electrolyte interface.[22,36,37] Figure 6e shows the R_{ct} for the two devices with Pt and CuS-3G CEs for applied voltages from 0 to 200 mV. The EIS measurements indicate that the R_{ct} of the CuS-3G composite cell is lower than that of the cell with Pt CE, which is mainly caused by the increase in the active catalytic surface area of the CuS-3G composite CE. These electrochemical measurements indicate that the CuS-3G composite CE shows superior electrocatalytic activity for electrolyte reduction, consistent with the similar FF for different devices. These results indicate that the CuS-3G nanocomposite CE on the glass substrate is comparable to that of the Pt CE on the FTO substrate.

An important aspect of solar cell research and development is high reproducibility without large batch-to-batch variations. Using

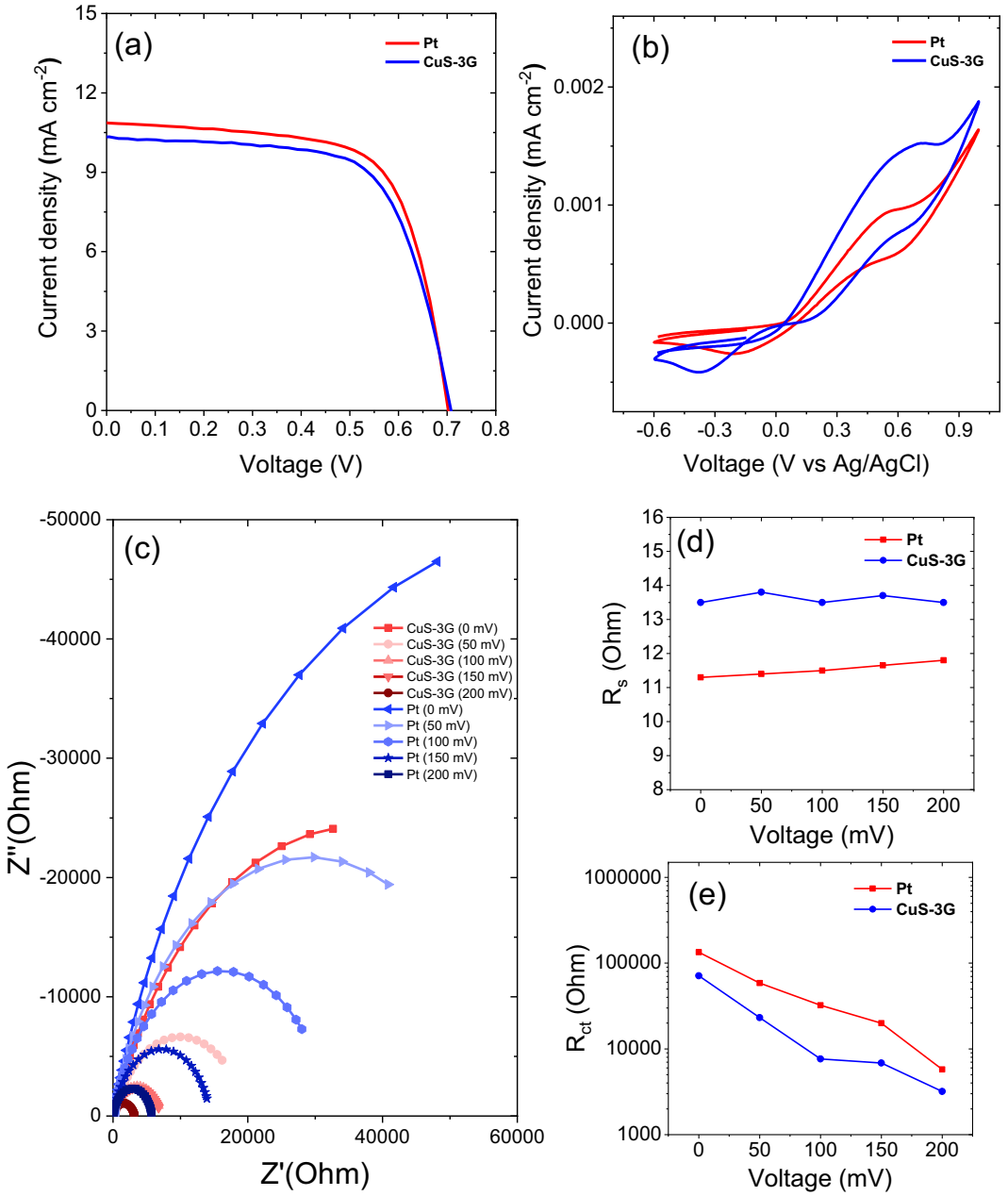

Figure 6. (a) Current density-voltage curves of solar cells under one sun simulated sunlight at AM 1.5G (100 mW cm^{-2}) fabricated using Pt and CuS-3G composite CEs, (b) cyclic voltammogram of Pt, and CuS-3G composite CEs. Electrochemical impedance spectroscopy analysis of the Pt and CuS-3G composite CEs for applied voltages of 0 to 200 mV: (c) Nyquist spectra; (d) series resistance (e) charge transfer impedance.

the same procedures as described previously for fabricating DSSCs based on the CuS-3G and Pt CEs, 12 independent devices were made over six different batches to ensure the repeatability and reproducibility of the results. Figure 7 presents the device performance parameters J_{sc}, V_{oc}, FF and PCE for all devices. These measurements show the remarkable reproducibility of our solar cells on the basis of similar functional parameters for cells within the different batches. The PV parameters for all devices based on the CuS-3G CEs are very similar, indicating that the new TCO and Pt free electrode is effective for fabrication of high-performance DSSCs with high reproducibility.

AFM is a useful technique to investigate surface morphology and topography. Figure 8 shows AFM images of the Pt and CuS-3G CEs. As can be seen in Figure 8b, the glass surface is fully covered with a dense crystalline grain layer of CuS. The rough structure with a high surface area is beneficial for the catalytic reaction.[18,32,36] The analysis of the images indicates that the roughness of the CuS-3G layer is 38 nm, which is more than two times higher than that of Pt (17 nm). This is supporting evidence that the electrocatalytic activity of CuS-3G can be comparable to that of Pt.

Conclusions

In conclusion, we have demonstrated a fast and highly reproducible solution processable approach to synthesize crystalline and uniform CuS-G nanocomposite thin films with different contents of graphene on glass substrates. XRD and XPS measurements verified the

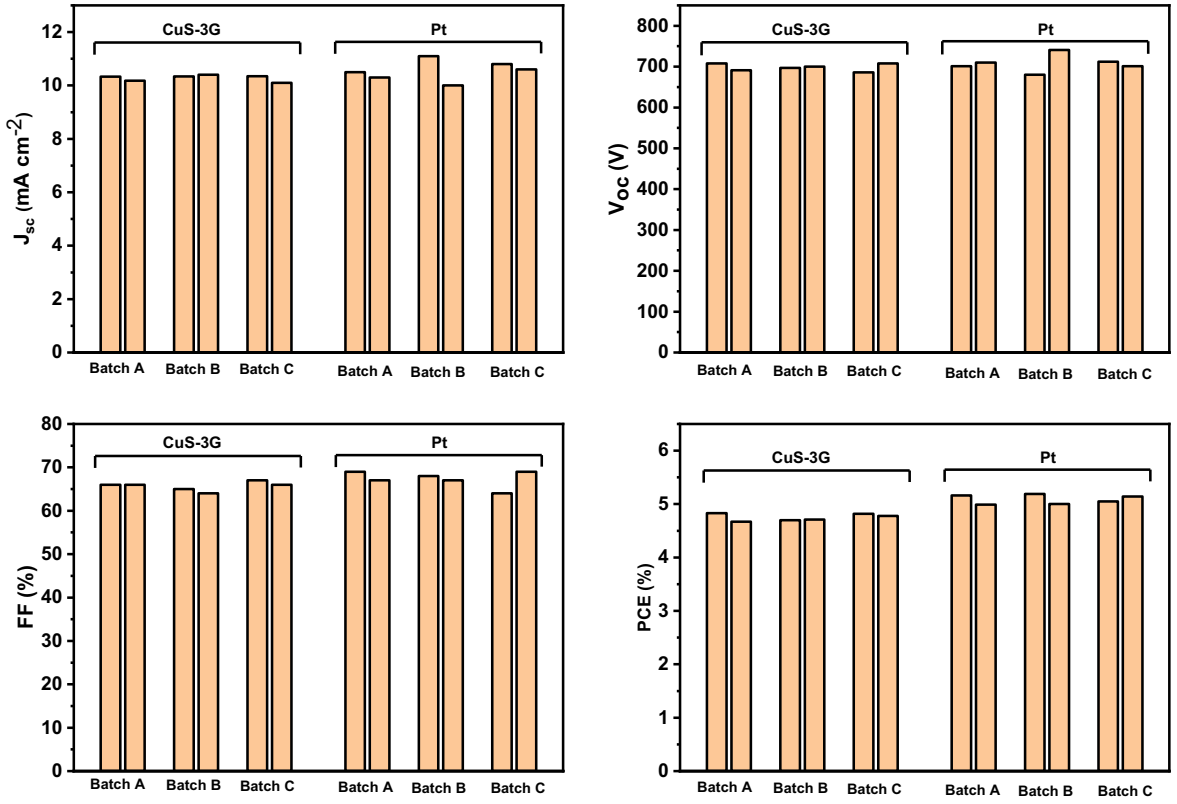

Figure 7. Device performance parameters of 12 devices collected over six different batches: (a) J_{sc} (mA.cm^{-2}); (b) V_{oc} (mV); (c) FF (%) and (d) PCE (%).

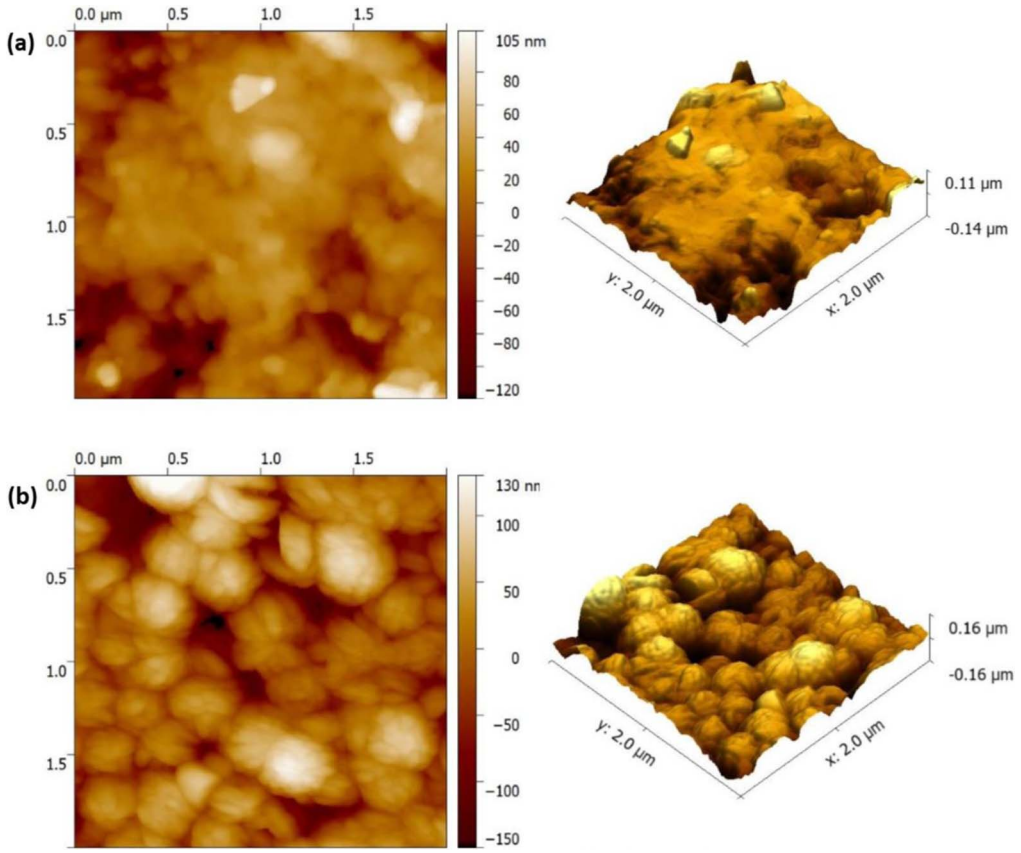

Figure 8. AFM images of: (a) Pt/FTO; (b) CuS-3G/Glass composite film.

structure and composition of the CuS-3G nanocomposite. As a proof of concept, as prepared CuS-3G nanocomposite thin films were found to exhibit good catalytic performance toward the reduction of the triiodide electrolyte, and exhibited an impressive PCE of 4.83% with high reproducibility under one sun simulated sunlight at AM 1.5G (100 mW cm^{-2}), which is comparable to that obtained using "standard" Pt CEs (5.14%). These results provide a low cost, simple and straightforward way to fabricate TCO and Pt free electrodes as a prospective candidate to replace highly expensive Pt-TCO CEs, due to its comparable catalytic properties and most importantly, the ease of fabrication at low temperatures.

Acknowledgments

We acknowledge funding from the Canada Foundation for Innovation for equipment and related operating funds and the Natural Science and Engineering Research Council (NSERC) of Canada for a Collaborative Research and Development project in partnership with MPB Technologies Inc. and Plasmionique Inc. F. R. is also supported by an NSERC Discovery grant and is grateful to the Canada Research Chairs program for funding and partial salary support. M. M. is thankful to Fonds de recherche du Québec-Nature et technologies (FRQNT) for a PhD Scholarship (B2X). G. S. S. and F. N. P. acknowledge the UNESCO Chair MATECSS for a PDF Excellence Scholarship and funding from the University of Electronic Science and Technology of China. F. R. acknowledges the government of China for a Chang Jiang Scholar short term award and Sichuan Province for a 1000 talents short term award. H. Zhao acknowledges the start funding support from Qingdao University and the funding from the Natural Science Foundation of Shandong Province (ZR2018MB001).

ORCID

Federico Rosei https://orcid.org/0000-0001-8479-6955

References

1. L. Suganthi and A. A. Samuel, *Renew. Sustain. Energy Rev.*, **16**, 1223 (2012).
2. M. Z. Iqbal and S. Khan, *Sol. Energy*, **160**, 130 (2018).
3. J. Wu, Z. Lan, J. Lin, M. Huang, Y. Huang, L. Fan, G. Luo, Y. Lin, Y. Xie, and Y. Wei, *Chem. Soc. Rev.*, **46**, 5975 (2017).
4. B. O'Regan and M. Gratzel, *Nature*, **353**, 737 (1991).
5. S. Tai, C. Liu, S. Chou, F. S. Chien, J. Lin, and T. W. Lin, *J. Mater. Chem.*, **22**, 24753 (2012).
6. Q. Tang, J. Duan, Y. Duan, B. He, and L. Yu, *Electrochim. Acta*, **178**, 886 (2015).
7. L. Heiniger, P. G. O. Brien, N. Soheilnia, Y. Yang, N. P. Kherani, M. Grätzel, G. A. Ozin, and N. Tétreault, *Adv. Mater.*, **25**, 5734 (2013).
8. K. Basu, H. Zhang, H. Zhao, S. Bhattacharya, F. Navarro-Pardo, P. K. Datta, L. Jin, S. Sun, F. Vetrone, and F. Rosei, *Nanoscale*, **10**, 15273 (2018).
9. K. Basu, D. Benetti, H. Zhao, L. Jin, F. Vetrone, A. Vomiero, and F. Rosei, *Sci. Rep.*, **6**, 1 (2016).
10. S. K. Matta, K. Kakiage, S. Makuta, A. Veamatahau, Y. Aoyama, T. Yano, M. Hanaya, and Y. Tachibana, *J. Phys. Chem. C*, **118**, 28425 (2014).
11. T. Daeneke, A. J. Mozer, Y. Uemura, S. Makuta, M. Fekete, Y. Tachibana, N. Koumura, U. Bach, and L. Spiccia, *J. Am. Chem. Soc.*, **134**, 16925 (2012).
12. S. Yun, Y. Liu, T. Zhang, and S. Ahmad, *Nanoscale*, **7**, 11877 (2015).
13. M. Mohammadnezhad, G. S. Selopal, Z. Wang, B. Stansfield, H. Zhao, and F. Rosei, *Chempluschem*, **83**, 682 (2018).
14. D. Benetti, T. Dembele, J. Benavides, H. Zhao, S. Cloutier, I. Concina, A. Vomiero, and F. Rosei, *J. Mater. Chem. C*, **4**, 3555 (2016).
15. G. S. Dembele, Kadiatou Therese Selopal, R. Milan, C. Trudeau, D. Benetti, A. Soudi, M. M. Natile, G. Sberveglieri, S. Cloutier, I. Concina, F. Rosei, and A. Vomiero, *J. Mater. Chem. A*, **3**, 2580 (2015).
16. K. T. Dembele, G. S. Selopal, C. Soldano, R. Nechache, J. C. Rimada, I. Concina, S. Giorgio, F. Rosei, and A. Vomiero, *J. Phys. Chem. C*, **117**, 14510 (2013).
17. K. T. Dembele, R. Nechache, L. Nikolova, A. Vomiero, C. Santato, S. Licoccia, and F. Rosei, *J. Power Sources*, **233**, 93 (2013).
18. S. Yun, P. D. Lund, and A. Hinsch, *Energy Environ. Sci.*, **8**, 3495 (2015).
19. Z. Tong, S. Liu, X. Li, J. Zhao, and Y. LI, *Nanoscale Horizons*, **3**, 261 (2018).
20. F. Navarro-Pardo, D. Benetti, J. Benavides, H. G. Zhao, S. G. Cloutier, V. M. Castano, A. Vomiero, and F. Rosei, *ECS J. of Solid State Sci. Technol.*, **6**, 32 (2017).
21. R. Akilimali, G. Singh, D. Benetti, I. Serrano-esparza, P. A. Algarabel, J. María, D. Teresa, Z. M. Wang, B. Stans, H. Zhao, and F. Rosei, *J. Power Sources*, **396**, 566 (2018).
22. G. Yue, J. Lin, S. Tai, Y. Xiao, and J. Wu, *Electrochim. Acta*, **85**, 162 (2012).
23. K. S. Lee, K. Lee, H. Wang, N. Park, Y. Lee, O. O. Park, and J. Hyeok, *Chem. Commun.*, **46**, 4505 (2010).
24. H. Kim, G. Veerappan, and J. H. Park, *Electrochim. Acta*, **137**, 164 (2014).
25. Z. Xu, T. Li, Q. Liu, F. Zhang, X. Hong, S. Xie, C. Lin, X. Liu, and W. Guo, *Sol. Energy Mater. Sol. Cells*, **179**, 297 (2018).
26. S. A. Patil, N. Mengal, A. Ali, S. Hoon, and H. Kim, *J. Alloy. Compd. J.*, **708**, 568 (2017).
27. X. Zhang, W. Guo, and C. Pan, *J. Mater. Chem. A*, **4**, 6569 (2016).
28. S. Thomas, T. G. Deepak, G. S. Anjusree, T. A. Arun, S. V. Nair, and A. S. Nair, *J. Mater. Chem. A*, **2**, 4474 (2014).
29. X. Miao, K. Pan, G. Wang, Y. Liao, L. Wang, and W. Zhou, *Chem. A Eur. J.*, **20**, 474 (2014).
30. X. Huang, Z. Zeng, Z. Fan, J. Liu, and H. Zhang, *Adv. Mater.*, **24**, 5979 (2012).
31. F. Navarro-Pardo, D. Benetti, H. Zhao, V. . Castano, A. Vomiero, and F. Rosei, *J. Power Sources*, **335**, 138 (2016).
32. Z. Shi, K. Deng, and L. Li, *Sci. Rep.*, **5**, 1 (2014).
33. W. Jarernboon, S. Pimanpang, S. Maensiri, E. Swatsitang, and V. Amornkitbamrung, *J. Alloys Compd.*, **476**, 840 (2009).
34. E. Palomares and J. N. Clifford, S. a Haque, T. Lutz and J. R. Durrant, *J. Am. Chem. Soc.*, **125**, 475 (2003).
35. A. Zaban, M. Greenshtein, and J. Bisquert, *ChemPhysChem*, **4**, 859 (2003).
36. C. Liu, S. Tai, S. Chou, Y. Yu, K. Chang, S. Wang, F. S.-S. Chien, J.-Y. Lin, and T.-W. Lin, *J. Mater. Chem.*, **22**, 21057 (2012).
37. S. A. Patil, P. Y. Kalode, R. S. Mane, D. V Shinde, A. Doyoung, C. Keumnam, M. M. Sung, S. B. Ambade, and S. Han, *Dalt. Trans.*, **43**, 5256 (2014).
38. Y. Zhang, J. Tian, H. Li, L. Wang, X. Qin, A. M. Asiri, A. O. Al-youbi, and X. Sun, *Langmuir*, **28**, 12893 (2012).
39. C. Ding, D. Su, W. Ma, Y. Zhao, D. Yan, and J. Li, *Appl. Surf. Sci.*, **403**, 1 (2017).
40. G. Nie, L. Zhang, X. Lu, X. Bian, W. Sun, and C. Wang, *Dalt. Trans.*, **42**, 14006 (2013).
41. K. Huang, J. Zhang, Y. Liu, and Y. Liu, *Int. J. Hydrogen Energy*, **40**, 10158 (2015).